Ti_nO_{2n-1} Magnéli phases studied using density functional theory

A. C. M. Padilha,[1,*] J. M. Osorio-Guillén,[1,2] A. R. Rocha,[3] and G. M. Dalpian[1,†]

[1]*Centro de Ciências Naturais e Humanas, Universidade Federal do ABC, Santo André, SP, Brazil*

[2]*Instituto de Física, Universidad de Antioquia UdeA, Calle 70 No. 52-51, Medellín, Colombia*

[3]*Instituto de Física Teórica, Universidade Estadual Paulista, São Paulo, SP, Brazil*

Defects in the rutile TiO_2 structures have been extensively studied, but the intrinsic defects of the oxygen-deficient Ti_nO_{2n-1} phases have not been given the same amount of consideration. Those structures, known as Magnéli phases, are characterized by the presence of ordered planes of oxygen vacancies, also known as shear planes, and it has been shown that they form conducting channels inside TiO-based memristor devices. Memristors are excellent candidates for a new generation of memory devices in the electronics industry. In this paper we present density-functional-theory–based electronic structure calculations for Ti_nO_{2n-1} Magnéli structures using PBESol+U ($0 \leqslant U \leqslant 5$ eV) and Heyd-Scuseria-Ernzerhof functionals, showing that intrinsic defects present in these structures are responsible for the appearance of states inside the band gap, which can act as intrinsic dopants for the enhanced conductivity of TiO_2 memristive devices.

PACS number(s): 71.20.Nr, 71.15.Mb

I. INTRODUCTION

Resistance switching in oxides has been known for over half a century [1–4], but attention to this phenomena has received a boost since the realization of the memristor, an idea that was originally formulated by Chua in the 1970s [5,6]. Williams *et al.* showed, by manufacturing, measuring, and switching the resistance state of such a device, basically an oxide thin film, that the memristance is a property that arises naturally at the nanoscale [7].

The working principle of the memristive-based memory device is the storage of information using the resistance state of a metal-insulator-metal structure. This in turn can be changed (write operation) and measured (read) when subjected to an electric field. The insulator layer is a nanometer-thick thin film, which can be composed of a wide variety of materials, such as binary oxides [8], perovskites [9–12], as well as many other compounds, which are known for their resistance switching properties [13,14].

The attractiveness of these devices for memory storage resides in the fact that they would be faster, denser, and less power consuming than those available today [15]. However, the mechanism for memristance is not, at present, well understood at the atomic level. Many authors point to a phase transition taking place inside the oxide matrix for TiO_2-based devices, leading to the formation of Magnéli phases (Ti_nO_{2n-1}, $n = 4,5$) conducting channels [16,17]. Those structures can be regarded as oxygen-deficient TiO_2, where the concentration of oxygen vacancies (V_O) is such that those defects become organized in a shear-plane structure. The formation of these extended defects is exemplified by the operation $(121)\frac{1}{2}[0\bar{1}1]$ in the rutile structure, where the first three indices refer to a plane in the rutile structure and the last three to a displacement vector in the same structure [18,19]. An example of this structure is presented in Fig. 1.

Despite the existence of many studies about defects in rutile TiO_2, both experimental [20–28] and theoretical [21,25], there are few works on the intrinsically defective Magnéli phases [29–35]. Electronic structure calculations have been used to understand mainly the Ti_2O_3 [32] and Ti_4O_7 [29–31]. Experimental reports [33–35] of some of these structures are not conclusive about the origin of the increase of electrical conductivity with respect to the rutile phase, nor about the switching mechanism. The question that arises is how the presence of extended-defect structures is related to the increase of electrical conductivity in this case.

Aiming to provide a general insight on the electronic structure of these oxygen-deficient oxides—which are known to exist—we present a systematic study based on *ab initio* density functional theory (DFT) electronic structure calculations for Ti_nO_{2n-1}, $2 \leqslant n \leqslant 5$. We used functionals based both on generalized gradient approximation (GGA) as well as on a hybrid approach (including part of the Hartree-Fock exchange contribution). On-site Coulomb interaction (DFT+U) for electrons in Ti(d) orbitals was also introduced, since there are questions as to the validity of using hybrid functionals in Ti-based oxides [36]. We show that these oxygen-deficient structures containing extended defects present localized states inside the gap, which in turn can act as intrinsic dopants to alter the transport properties of memristive devices.

II. SIMULATION DETAILS

Simulations were performed using the Vienna *ab initio* software package (VASP) [37–40], within the projector augmented waves scheme [41,42]. The GGA functional PBESol [43], with and without on-site Coulomb interaction (within Dudarev's approach [44]) for Ti(d) orbitals, and hybrid Heyd-Scuseria-Ernzerhof (HSE) [45] (20% HF exchange) were used for ionic relaxations (forces $< 2.5 \times 10^{-3}$ eV/Å) and orbital projected density of states (PDOS) calculations. The values of U (in fact, using Dudarev's method, only U-J is used, where J is the spherically averaged matrix element of the screened Coulomb interaction between electrons. Hence, for all calculations, we used $J = 0$) used for the on-site interaction

*antonio.padilha@ufabc.edu.br
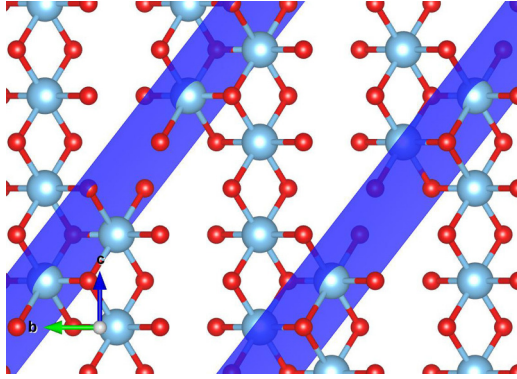
†gustavo.dalpian@ufabc.edu.br

FIG. 1. (Color online) Cut of the Magnéli structure generated through the operation $(121)\frac{1}{2}[0\bar{1}1]$. The shear planes (121) are featured in blue.

ranged from 0–5 eV. For all structures spin polarization was taken into account. Monkhorst-Pack sampling was used for ionic relaxation with the GGA functional and Γ-centered meshes for PDOS calculations after that, using an energy cutoff of 520 eV. For the hybrid functional calculations, only Γ-centered meshes were used for both relaxation and PDOS, with a smaller cutoff (400 eV), in such a manner that the k points would be more equally spaced in all directions. Finally the $3p3d4s$ and $2s2p$ configurations were considered as valence electrons for Ti and O atoms respectively.

The use of the Hubbard U parameter resulted in a change of the electronic structure when the system was driven from the delocalized regime (GGA functional calculation, $U = 0$) that neglects the orbital dependence of the Coulomb interaction, to the regime where orbital dependence is included, ($U > 0$) leading to a better description of localized states (Ti(d) orbitals). We used values for U that ranged from 0–5 eV, but we report only the meaningful results for $U = 0$ and 5 eV.

When possible, unit cell symmetry was used to obtain the primitive unit cell from crystallographic data using the PHONOPY software [46]. All crystal structure images were generated using the VESTA software [47].

III. RESULTS

A. Structural properties

Table I lists the space groups for all structures studied in this work. From x-ray diffraction experiments [48,49], it is known

TABLE I. Space group in the international and Schoenfiles notations for all Ti_nO_{2n-1}, ($2 \leqslant n \leqslant 5$ for the structures used in this work) after ionic relaxation.

	Space Group	
	International (#)	Schoenflies
Ti_2O_3	$R\bar{3}c$ (167)	D_{3d}
α-Ti_3O_5	$Cmcm$ (63)	D_{2h}
β-Ti_3O_5	$C2/m$ (12)	C_{2h}
γ-Ti_3O_5	$C2/c$ (15)	C_{2h}
Ti_4O_7	$P\bar{1}$ (2)	C_i
Ti_5O_9	$P1$ (1)	C_1

that Ti_2O_3 presents a rhombohedral corundum-like structure with space group $R\bar{3}c$ where the Ti atoms are enclosed by oxygen in an octahedral format. These polyhedra are the building blocks of this structure, as well as all the other structures presented here, and hereafter will be referred to as TiO_6 octahedra. For Ti_2O_3, these building blocks are displaced in face-sharing pairs.

The Ti_3O_5 structure obtained from crystallographic databases was not unique. The three phases, α (orthorhombic, anosovite-like, group $Cmcm$) [50], β (monoclinic, group $C2/m$) [51,52], and γ-Ti_3O_5 (monoclinic, $I2/c$)[53] were used for the calculations. Onoda *et al.* pointed out a first-order phase transition at approximately 440–460 K [54] between α and β-Ti_3O_5. The transition from β to the room-temperature γ phase at $\approx$250 K was reported by Hong and Åsbrink [53].

Ti_4O_7 presents a Magnéli structure composed, as described in the other structures, by TiO_6 octahedra for all the three phases characterized by Marezio *et al.* [55–57]. This structure can be viewed as infinite planes of rutile, n-TiO_6 octahedra thick along the (121) direction of the rutile crystal, limited by a plane of defects (oxygen vacancies), which characterizes a crystallographic shear structure [19,29]. The unit cells obtained from crystallographic databases were triclinic and presented space group $P\bar{1}$ for the three known phases: high- (HT), intermediate- (IT), and low-temperature (LT). The only difference between those structures was a slight displacement of the atoms, whose positions became essentially equal after ionic relaxation. This also has lead to identical PDOS in all cases. Because of that, we present only the results for the relaxation using the LT phase as a starting configuration in Table II.

Finally, Ti_5O_9 belongs to the same Magnéli series (Ti_nO_{2n-1}), presenting a triclinic unit cell. The difference is that the rutile-like planes are one extra unit of TiO_6 thicker. The initial structure used for our calculations was obtained by Andersson [18].

The structural parameters, after relaxation, for all oxides studied in this work are listed on Table II. The difference between experimental and calculated lattice parameters was lower than 6% for all structures and both functionals, and it was not possible to notice any systematic underestimation or overestimation of the values regarding the functional chosen for the simulations.

B. Electronic and magnetic properties

Orbital-projected density of states (PDOS) and magnetization profiles $[\mu(\vec{r}) = \rho_\uparrow(\vec{r}) - \rho_\downarrow(\vec{r})]$ were obtained for all systems using both PBESol+U ($0 \leqslant U \leqslant 5$ eV) and HSE functionals. It is a characteristic of GGA functionals to underestimate the band gap, while calculations using hybrid functionals frequently result in better agreement with experimental data for some oxides [58]. The use of the Hubbard U parameter presents a better description of the localization of d orbital electrons in transition metals oxides, which is exactly the case of the structures studied in this work.

The positioning of Ti_nO_{2n-1} defect levels is a key ingredient to determine the electrical conductivity—specifically its enhancement in memristive devices—of these structures. Thus we used both methodologies to study the electronic structure of these defect levels.

TABLE II. Experimental and theoretical values of lattice parameters for the Ti$_2$O$_3$, α, β, and γ-Ti$_3$O$_5$, Ti$_4$O$_7$, and Ti$_5$O$_9$ structures. Mean absolute relative error for unit cell volume is also presented in parenthesis. Values presented are those of the primitive cells.

			a(Å)	b(Å)	c(Å)	α(°)	β(°)	γ(°)	Ω (Å³)
Ti$_2$O$_3$		Exp [48,49]	5.433	–	–	56.57	–	–	160.37
		PBESol	5.471	–	–	54.89	–	–	163.80 (2.14%)
		HSE	5.370	–	–	57.62	–	–	154.87 (3.43%)
Ti$_3$O$_5$	α	Exp [50]	3.747	5.090	9.715	90.00	90.00	68.40	172.27
		PBESol	3.760	5.237	9.937	90.00	90.00	68.96	182.60 (6.00%)
		HSE	3.682	5.258	9.978	90.00	90.00	69.50	180.94 (5.03%)
	β	Exp [51]	3.802	5.233	9.442	91.79	90.00	111.30	174.94
		PBESol	3.834	5.195	9.215	90.87	90.00	111.65	170.60 (2.48%)
		HSE	3.791	5.196	9.173	90.76	90.00	111.40	168.23 (3.61%)
	γ	Exp [53]	5.075	5.658	7.181	109.58	90.00	116.64	170.85
		PBESol	4.997	5.627	7.180	109.81	90.00	116.36	167.45 (1.99%)
		HSE	5.076	5.664	7.069	109.36	90.00	116.62	168.76 (1.22%)
Ti$_4$O$_7$		Exp [55]	5.626	6.892	7.202	63.71	109.68	105.24	233.60
		PBESol	5.569	6.868	7.092	64.22	109.72	104.91	229.12 (1.92%)
		HSE	5.618	6.898	7.076	63.77	108.77	104.23	231.09 (1.07%)
Ti$_5$O$_9$		Exp [18]	5.569	7.120	8.865	97.55	112.34	108.50	295.33
		PBESol	5.558	7.110	8.846	97.75	112.51	108.61	292.54 (0.94%)
		HSE	5.550	7.040	8.763	96.96	112.35	108.09	289.68 (1.91%)

The PBESol calculations resulted in a metallic behavior. It is evident from the Ti$_2$O$_3$ PDOS in Fig. 2 that some states, mainly composed of Ti(d) orbitals, move away from the unoccupied levels as the parameter U is increased, reaching the same qualitative results as in the HSE case for $U = 5$. This effect was expected owing to the better description, compared to GGA, of d orbitals by hybrid functionals [59] as well as the more localized character of these orbitals with respect to increasing U. These levels can be interpreted as a defectlike level inherent to the crystalline structure, which can be split from the other Ti(d) states that are unoccupied with increasing U.

Experimental E_g for this structure is 1 eV [60], which is in excellent agrement with the results using PBESol+U, $U = 5$ eV, and HSE, given that the band gap is interpreted as the energy difference between the defect levels and the CBM in Fig. 2.
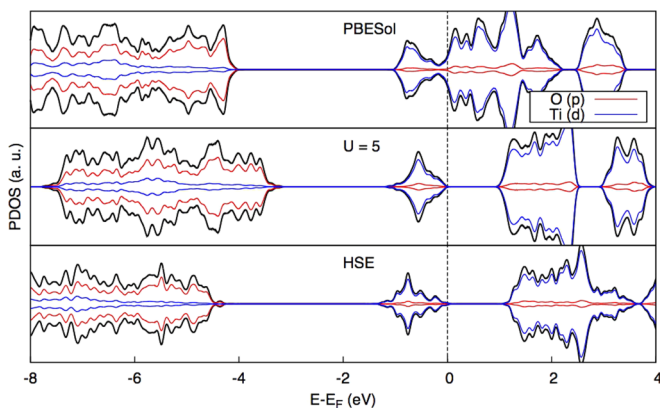

FIG. 2. (Color online) Ti$_2$O$_3$ PDOS obtained with PBESol functional (top), PBESol+U (middle panel), and HSE (bottom).

In the case of Ti$_3$O$_5$, some states—mainly of Ti(d) character—were split from the unoccupied levels, leading to the formation of defect levels inside the band gap when used $U = 5$, while for HSE calculations, some states remained very close to the Fermi energy, leading to a metalliclike character for β- and γ-Ti$_3$O$_5$ (Fig. 3). According to Rao *et al.* [61] and Bartholomew and Frankl [33], this system is a semiconductor for temperatures below $\approx$400 K, therefore the description of the room-temperature phase γ-Ti$_3$O$_5$ as a metal by HSE is by no means correct.

As previously discussed, total energy, PDOS (Fig. 4) and magnetization were essentially equal for LT, IT and HT-Ti$_4$O$_7$ calculations using PBESol functional. This was expected since DFT calculations always take place at $T = 0$ K leading the system to relax to the LT structure in all three cases. Calculations with HSE showed that the magnetic ordering is dependent on initial conditions, although it does not influence the final atomic arrangement. The presence of magnetization in these structures leads to a lower-energy configuration, a fact that was confirmed with calculations without spin polarization, which resulted in higher total energies.

Similar results were obtained for Ti$_5$O$_9$ (Fig. 5), but one striking difference was the depth of the defectlike levels in this case: about 1.8 eV lower than the CBM with the HSE functional. It is also worth pointing out that for this system, HSE gives different descriptions for Ti$_4$O$_7$ and Ti$_5$O$_9$. The first seems to be a half metal whereas the former does not.

The main result used to decide which methodology between hybrid approach and the use of the Hubbard U parameter is better suited to study these systems is the agreement of the band gap obtained through the calculations with the experimental one. This task, which in principle seems quite straightforward, is not simple for the two structures of interest for memristor applications, the Ti$_4$O$_7$ or the Ti$_5$O$_9$. For the former, there is
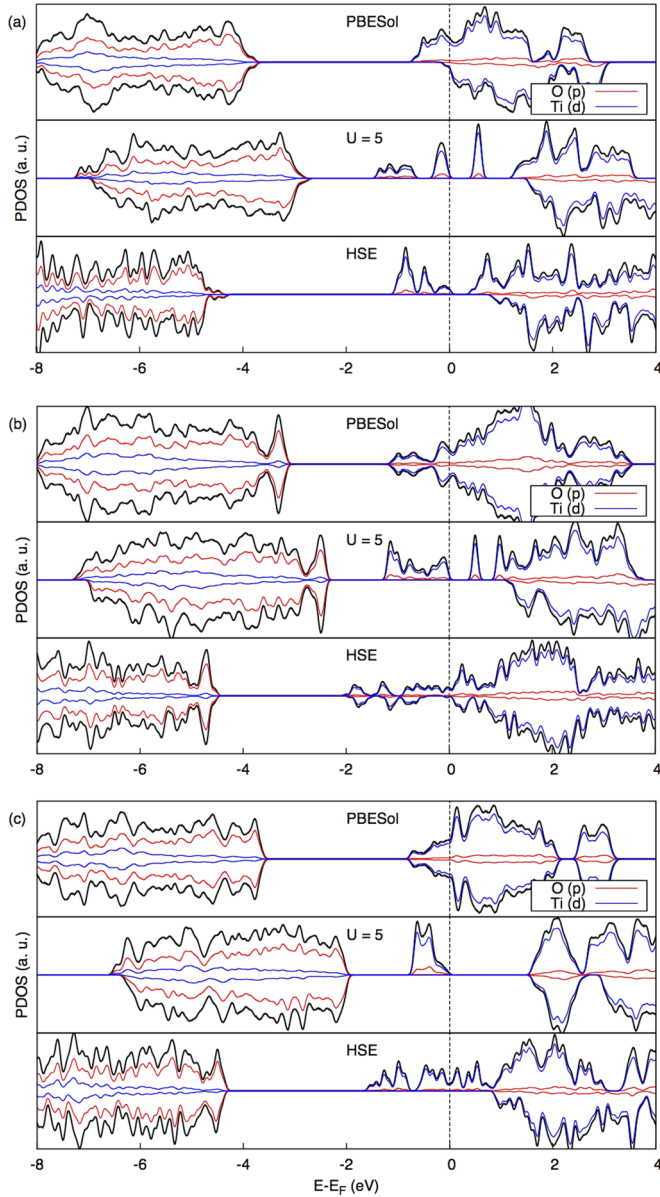
FIG. 3. (Color online) (a) α-, (b) β-, and (c) γ-Ti_3O_5 PDOS obtained with PBESol functional (top), PBESol+U (middle), and HSE (bottom).
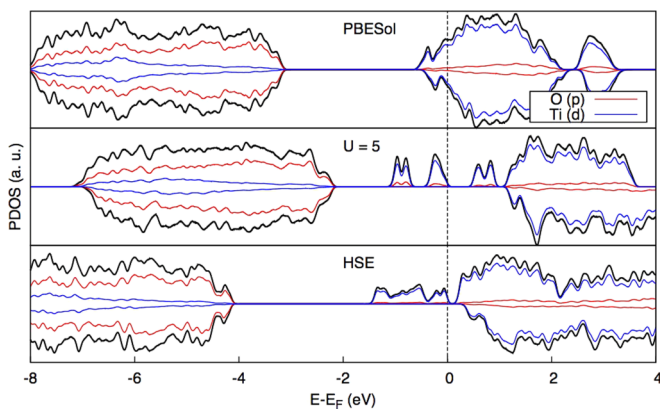

FIG. 4. (Color online) Ti_4O_7 PDOS obtained with PBESol functional (top), PBESol+U (middle), and HSE (bottom).
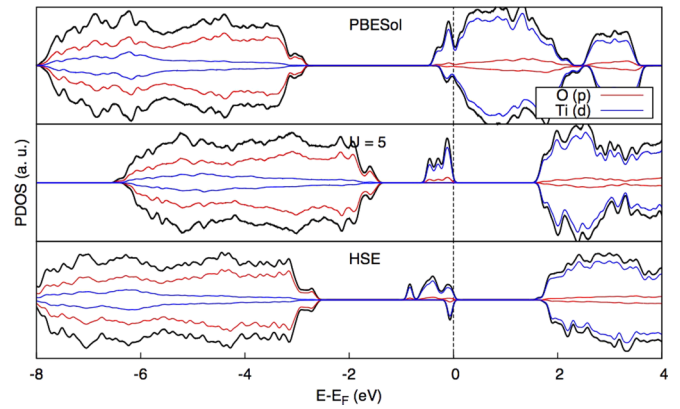

FIG. 5. (Color online) Ti_5O_9 PDOS obtained with PBESol functional (top), PBESol+U (middle), and HSE (bottom).
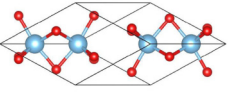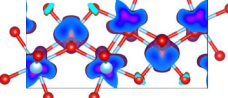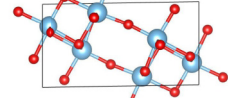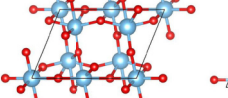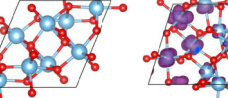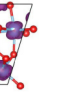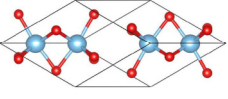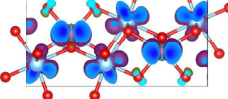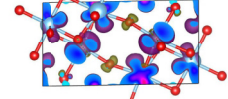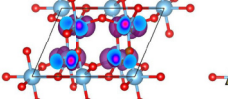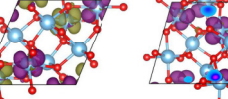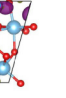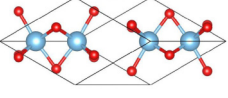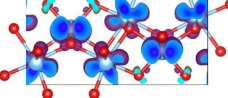
no conclusive experimental data on the band-gap energy and for the latter, as to our knowledge, no reports at all. The band gap of Ti_4O_7 is reported to be 0.041 eV from conductivity measurements [62], 0.6 eV from spectroscopy data [63], and 0.25 eV from optical transmission data [64]. In principle, both HSE and $U = 5$ result in compatible band gaps. Although the DFT+U is not designed to increase the band gap, it is a consequence of the localization of the d orbitals when this methodology is used.
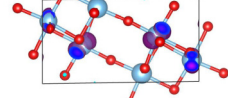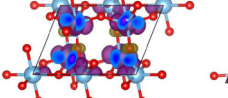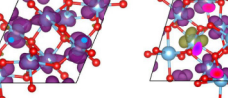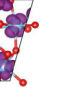
The magnetization for all structures was higher for $U = 5$ eV as well as HSE functional calculations compared to GGA alone, with the exception of Ti_2O_3. These results are shown in Table III. As is known for the same type of defects (V_O's) in the TiO_2 rutile, the removal of oxygen atoms from the oxide structure leaves a pair of unbound electrons [36,65]. Each of the Ti_nO_{2n-1} phases presents two V_O's per unit cell, therefore there are four electrons left behind. Magnetization density plots for Ti_nO_{2n-1}, $2 \leqslant n \leqslant 5$ are also shown in Table III, where it is possible to identify these electrons laying on the $Ti(d)$ orbitals through the unit cell. They are also responsible for the defect levels inside the band gap seen in all structures.

The band decomposed charge density for both Ti_2O_3 and Ti_4O_7 defect levels are presented in Table IV. In those plots it is possible to notice that both U and HSE were responsible for a better localization of these levels, which are clearly of $Ti(d)$ character, presenting apparently the same hybridization with $O(p)$ orbitals in both cases. This hybridization could be a problem, as pointed out in the literature, in the case of MnO polymorphs [66], where GW calculations where used as a benchmark for the correct ordering of $Mn(d)$ levels. We could in principle follow the same path, but due to computational cost, we decided only to report those defect levels, and point out that they could be responsible for n-doping in these structures, which could be a possible explanation for their enhanced conductivity on memristors.

One possible interpretation for the differences between the PBESol+U and HSE results for the β-, γ-Ti_3O_5 and Ti_4O_7 is that both methods are known to present improvements to the electronic structure in this kind of system, but in different ways. The first uses the fact that the on-site Coulomb interaction (which in this case is inserted in the system through a Hubbard parameter) is responsible for the localization of

TABLE III. (Color online) Total magnetization per unit cell (Ti atom) in units of Bohr magnetons (μ_B) and respective magnetization density ($\mu(\vec{r}) = \rho_\uparrow(\vec{r}) - \rho_\downarrow(\vec{r})$) plots over the unit cell for all Ti$_n$O$_{2n-1}$ structures presented in this work obtained with PBESol, $U = 5$, and HSE functionals.

	Ti$_2$O$_3$	Ti$_3$O$_5$ α	Ti$_3$O$_5$ β	Ti$_3$O$_5$ γ	Ti$_4$O$_7$	Ti$_5$O$_9$
PBESol						
	-0.06 (-0.01)	3.75 (0.62)	0.00 (0.00)	0.15 (0.02)	1.12 (0.14)	2.19 (0.22)
$U = 5$						
	0.00 (0.00)	4.00 (0.67)	3.99 (0.66)	4.00 (0.67)	4.00 (0.50)	4.00 (0.40)
HSE						
	0.00 (0.00)	4.00 (0.67)	0.94 (0.16)	4.00 (0.67)	4.00 (0.50)	2.75 (0.27)

Ti(d) electrons, which in turn leads to a better description of these orbitals. The hybrid approach relies on the fact that through the insertion of part of Hartree-Fock exchange in the exchange-correlation functional, there is a partial cancellation of the self interaction, considered as an intrinsic problem in GGA-based calculations [67]. Those different approaches seem to play a decisive role in the final electronic structure of the systems being studied, as could be seen in the different total magnetizations for these two structures, but qualitatively their description of the position of the defect levels and their character is very similar. It is important to notice that the HSE calculations led to a metallic state for β- and γ-Ti$_3$O$_5$, while for all other structures, a semiconductor PDOS was obtained (it was possible to notice the separation between occupied and unoccupied levels). This same semiconducting behavior was obtained using the Hubbard U parameter. According to Rao *et al.* [61] and Bartholomew and Frankl [33], the systems studied in this work are all semiconductors for temperatures below 100 K. These results seem reasonable, given that DFT calculations always take place at $T = 0$ K.

TABLE IV. (Color online) Band decomposed charge-density plots over the unit cell over the defect levels for Ti$_2$O$_3$ and Ti$_4$O$_7$ using PBESol, PBESol+U ($U = 5$ eV), and HSE functionals.

	PBESol	U = 5	HSE
Ti$_2$O$_3$			
Ti$_4$O$_7$			
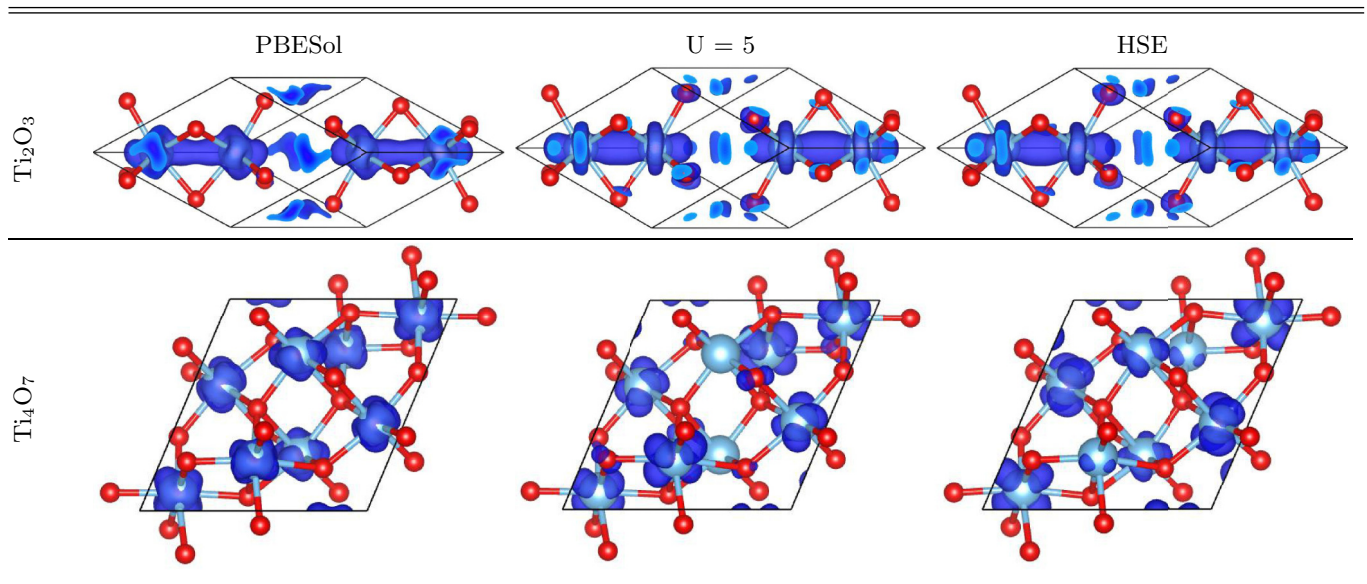
In the case of Ti_2O_3, the magnetization is very weak and present only on PBESol calculations. When U was introduced, it becomes negligible, and the same physical interpretation can be given: a better description of the localization of Ti(d) orbitals. The same behavior of $U = 5$ is seen when the HSE functional is used, with the exception of β-Ti_3O_5 and Ti_5O_9. This could be understood as observations of different local minima related to the different magnetic configurations. In fact, we performed other calculations for different magnetic orderings for all structures except Ti_5O_9 and a difference of few meV was found between the total energy per unit cell without any restriction on the magnetic moments (shown in Table III) and restricting the initial configuration to antiferromagnetic (AF) $\mu = 0$ configurations for Ti(d) electrons. This points out that those structures present a number of minima of the total energy with respect to magnetic ordering, but the difference is relatively small. In any case, it is clear that the localization is more pronounced in either situation.

IV. CONCLUSION

In this work we showed that DFT-based calculations are able to point out defect levels inside the band-gap region for all Ti_nO_{2n-1}, $2 < n < 5$. Those defects, in the same way as defects on rutile TiO_2, are mainly of Ti(d) character and exist because of the introduction of intrinsic V_O's in the structure. Those levels are either close or attached to the CBM when GGA functionals are used for calculations, but a better description of Ti(d) orbitals—through the Hubbard U parameter, or a hybrid functional—can lead to the positioning of these levels away from the CBM, as shallow or even deep levels. Although we find an extended defect level, forming a narrow band, which has a local magnetic moment, the value of the exchange coupling J is very small (at least for the different configurations tried).

The enhancement of the electronic conductivity observed for these oxides with respect to rutile could be explained, in principle, by the presence of these defects close to the CBM, which play the role of intrinsic dopants in these systems. This fact should be important in order to better understand the memristive devices. Similarities between the electronic structures around the CBM and with respect to the defect levels obtained with PBESol+U, $U = 5$, and HSE are remarkable for the Ti_2O_3, Ti_4O_7, and Ti_5O_9. The Ti_3O_5 on the other hand has a metallic character for HSE, while for PBESol+U, $U = 5$, a band gap appeared.

A comparison between the PBESol+U and HSE functionals was also presented, aiming to identify which of the two methodologies is best suited for the study of correlated oxide systems, as the Ti_nO_{2n-1} Magnéli structures presented in this work. While the total magnetization results were not equal for all structures, the localization and character of the defect levels were similarly described with both methods. The fact that HSE calculations result in metallic behavior for two of the systems studied, which were all semiconductors according to PBESol+U calculations, while experimental evidence points out a semiconductor behavior, is an evidence that the latter methodology could be best suited for this kind of system.

[1] T. W. Hickmott, J. Appl. Phys. **33**, 2669 (1962).

[2] K. L. Chopra, J. Appl. Phys. **36**, 184 (1965).

[3] F. Argall, Sol. State Elec. **11**, 535 (1968).

[4] O. W. Johnson, Appl. Phys. Lett. **13**, 338 (1968).

[5] L. O. Chua, IEEE Trans. Circ. Theo. CT **18**, 507 (1971).

[6] L. O. Chua and S. M. Kang, Proc. IEEE **64**, 209 (1976).

[7] D. B. Strukov, G. S. Snider, D. R. Stewart, and R. S. Williams, Nature (London) **453**, 80 (2008).

[8] K. Szot, M. Rogala, W. Speier, Z. Klusek, A. Besmehn, and R. Waser, Nanotechnology **22**, 254001 (2011).

[9] R. Muenstermann, T. Menke, R. Dittmann, and R. Waser, Adv. Mat. **22**, 4819 (2010).

[10] K. Szot, W. Speier, G. Bihlmayer, and R. Waser, Nat. Mater. **5**, 312 (2006).

[11] A. Beck, J. G. Bednorz, Ch. Gerber, C. Rossel, and D. Widmer, Appl. Phys. Lett. **77**, 139 (2000).

[12] C. Rossel, G. I. Meijer, D. Brémaud, and D. Widmer, J. Appl. Phys. **90**, 2892 (2001).

[13] R. Waser and M. Aono, Nat. Mater. **6**, 833 (2007).

[14] Y. Hirose, J. Appl. Phys. **47**, 2767 (1976).

[15] D. S. Jeong, R. Thomas, R. S. Katiyar, J. F. Scott, H. Kohlstedt, A. Petraru, and C. S. Hwang, Rep. Progr. Phys. **75**, 076502 (2012).

[16] D.-H. Kwon, K. M. Kim, J. H. Jang, J. M. Jeon, M. H. Lee, G. H. Kim, X.-S. Li, G.-S. Park, B. Lee, S. Han, M. Kim, and C. S. Hwang, Nat. Nanotech. **5**, 148 (2010).

[17] G. Hwan Kim, J. Ho Lee, J. Yeong Seok, S. Ji Song, J. Ho Yoon, K. Jean Yoon, M. Hwan Lee, K. Min Kim, H. Dong Lee, S. Wook Ryu, T. Joo Park, and C. S. Hwang, Appl. Phys. Lett. **98**, 262901 (2011).

[18] S. Andersson, D. H. Templeton, S. Rundqvist, E. Varde, and G. Westin, Acta Chem. Scand. **14**, 1161 (1960).

[19] S. Harada, K. Tanaka, and H. Inui, J. Appl. Phys. **108**, 083703 (2010).

[20] V. Henrich, G. Dresselhaus, and H. Zeiger, Phys. Rev. Lett. **36**, 1335 (1976).

[21] M. Nolan, S. D. Elliott, J. S. Mulley, R. A. Bennett, M. Basham, and P. Mulheran, Phys. Rev. B **77**, 235424 (2008).

[22] W. Göpel, and J. A. Anderson, D. Frankel, M. Jaehnig, K. Phillips, J. A. Schäfer, and G. Rocker, Surf. Sci. **139**, 333 (1984).

[23] M. A. Henderson, W. S. Epling, C. H. F. Peden, and C. L. Perkins, J. Phys. Chem. B **107**, 534 (2003).

[24] S. Yang, L. E. Halliburton, A. Manivannan, P. H. Bunton, D. B. Baker, M. Klemm, S. Horn, and A. Fujishima, Appl. Phys. Lett. **94**, 162114 (2009).

[25] S. Wendt, P. T. Sprunger, E. Lira, G. K. H. Madsen, Z. Li, J. O. Hansen, J. Matthiesen, A. Blekinge-Rasmussen, E. Laegsgaard, B. Hammer, and F. Besenbacher, Science **320**, 1755 (2008).

[26] K. Mitsuhara, H. Okumura, A. Visikovskiy, M. Takizawa, and Y. Kido, J. Chem. Phys. **136**, 124707 (2012).

[27] C. M. Yim, C. L. Pang, and G. Thornton, Phys. Rev. Lett. **104**, 036806 (2010).

[28] P. Kruger, J. Jupille, S. Bourgeois, B. Domenichini, A. Verdini, L. Floreano, and A. Morgante, Phys. Rev. Lett. **108**, 126803 (2012).

[29] L. Liborio, G. Mallia, and N. Harrison, Phys. Rev. B **79**, 245133 (2009).

[30] M. Weissmann and R. Weht, Phys. Rev. B **84**, 144419 (2011).

[31] I. Leonov, A. N. Yaresko, V. N. Antonov, U. Schwingenschlögl, V. Eyert, and V. I. Anisimov, J. Phys.: Condens. Matter **18**, 10955 (2006).

[32] Y. Guo, S. J. Clark, and J. Robertson, J. Phys.: Condens. Matter **24**, 325504 (2012).

[33] R. Bartholomew and D. Frankl, Phys. Rev. **187**, 828 (1969).

[34] A. D. Inglis, Y. L. Page, P. Strobel, and C. M. Hurd, J. Phys. C: Solid State Phys. **16**, 317 (1983).

[35] R. L. Clarke and S. K. Harnsberger, Am. Lab. **20**, 8 (1988).

[36] A. Janotti, J. B. Varley, P. Rinke, N. Umezawa, G. Kresse, and C. G. VandeWalle, Phys. Rev. B **81**, 085212 (2010).

[37] G. Kresse and J. Hafner, Phys. Rev. B **47**, 558 (1993).

[38] G. Kresse and J. Hafner, Phys. Rev. B **49**, 14251 (1994).

[39] G. Kresse, Comp. Mat. Sci. **6**, 15 (1996).

[40] G. Kresse and J. Furthmüller, Phys. Rev. B **54**, 11169 (1996).

[41] P. E. Blöchl, Phys. Rev. B **50**, 17953 (1994).

[42] G. Kresse and D. Joubert, Phys. Rev. B **59**, 1758 (1999).

[43] J. P. Perdew, A. Ruzsinszky, G. I. Csonka, O. A. Vydrov, G. E. Scuseria, L. A. Constantin, X. Zhou, and K. Burke, Phys. Rev. Lett. **100**, 136406 (2008).

[44] S. L. Dudarev, G. A. Botton, S. Y. Savrasov, C. J. Humphreys, and A. P. Sutton, Phys. Rev. B **57**, 1505 (1998).

[45] J. Heyd, G. E. Scuseria, and M. Ernzerhof, J. Chem. Phys. **118**, 8207 (2003).

[46] A. Togo, F. Oba, and I. Tanaka, Phys. Rev. B **78**, 134106 (2008).

[47] K. Momma and F. Izumi, J. Appl. Cryst. **44**, 1272 (2011).

[48] W. R. Robinson, J. Sol. St. Chem. **9**, 255 (1974).

[49] S. Abrahams, Phys. Rev. **130**, 2230 (1963).

[50] A. A. Rusakov and G. S. Zhdanov, Doklady Akademii Nauk SSSR **77**, 411 (1951).

[51] S. Åsbrink and A. Magnéli, Acta Cryst. **12**, 575 (1959).

[52] I. Grey, C. Li, and I. Madsen, J. Sol. Stat. Chem. **113**, 62 (1994).

[53] S.-H. Hong and S. Åsbrink, Acta Cryst. B **38**, 2570 (1982).

[54] M. Onoda, J. Sol. State Chem. **136**, 67 (1998).

[55] Y. Le Page and M. Marezio, J. Sol. State Chem. **53**, 13 (1984).

[56] M. Marezio, D. McWhan, P. Dernier, and J. Remeika, J. Sol. State Chem. **6**, 213 (1973).

[57] M. Marezio and P. Dernier, J. Sol. State Chem. **3**, 340 (1971).

[58] C. Di Valentin, G. Pacchioni, and A. Selloni, Phys. Rev. Lett. **97**, 166803 (2006).

[59] F. Tran, P. Blaha, K. Schwarz, and P. Novák, Phys. Rev. B **74**, 155108 (2006).

[60] M. Uchida, J. Fujioka, Y. Onose, and Y. Tokura, Phys. Rev. Lett. **101**, 066406 (2008).

[61] C. Rao, S. Ramdas, R. Loehman, and J. Honig, J. Sol. St. Chem. **3**, 83 (1971).

[62] L. N. Mulay and W. J. Danley, J. Appl. Phys. **41**, 877 (1970).

[63] M. Abbate, R. Potze, G. A. Sawatzky, C. Schlenker, H. J. Lin, L. H. Tjeng, C. T. Chen, D. Teehan, and T. S. Turner, Phys. Rev. B **51**, 10150 (1995).

[64] D. Kaplan, C. Schlenker, and J. J. Since, Phil. Mag. **36**, 1275 (1977).

[65] H.-Y. Lee, S. J. Clark, and J. Robertson, Phys. Rev. B **86**, 075209 (2012).

[66] H. Peng and S. Lany, Phys. Rev. B **87**, 174113 (2013).

[67] Y.-S. Kim, K. Hummer, and G. Kresse, Phys. Rev. B **80**, 035203 (2009).